Controlling the Morphology of ZnO Nanostructures in a Low-Temperature Hydrothermal Process

U. Pal*,† and P. Santiago‡

Instituto de Física, Universidad Autónoma de Puebla, Apdo. Postal J-48, Puebla, Pue. 72570, Mexico, and Instituto de Física, Universidad Nacional Autónoma de México, A.P. 20-365, C.P. 01000 Mexico D.F., Mexico

Received: May 12, 2005; In Final Form: June 20, 2005

ZnO nanostructures of different morphologies were grown in a controlled manner using a simple low-temperature hydrothermal technique. Controlling the content of ethylenediamine (soft surfactant) and the pH of the reaction mixture, nanoparticles, nanorods, and flowerlike ZnO structures could be synthesized at temperatures 80−100 °C with excellent reproducibility. High-resolution electron microscopy revealed the well crystalline nature of all the nanostructures with preferential growth along the [002] direction for linear structures. Photoluminescence spectra of the as-grown nanostructures revealed oxygen-vacancy-related defects in them, which could be reduced by air annealing at 250 °C. Possible mechanisms for the variation of morphology with synthesis parameters are discussed.

Introduction

Semiconductor nanostructures with controlled dimension and morphology are critical for the fabrication of optoelectronic devices. Among the promising optoelectronic semiconductors, ZnO with a direct wide band gap (3.37 eV) and large excitation binding energy (60 meV),[1] is one of the most important functional materials exhibiting near-UV emission,[2] gas and piezoelectric sensing,[3,4] and has potentials for fabrication of several other functional nanodevices.[5−8]

Several high-temperature growth techniques such as vapor-phase transport (VPT),[9] vapor−liquid−solid (VLS) growth,[10−13] vapor-phase epitaxy,[14] template-assisted growth,[15] along with some low-temperature growth techniques such as chemical reactions from aqueous solutions,[16−18] and electrochemical techniques[19,20] have been used for the synthesis of ZnO nanostructures. Generally, the growth of nanostructures requires complicated equipments, if epitaxial techniques are used and/or elaborate preparation of source and substrate materials if catalysis and chemical reactions are involve in the process.[21] Catalyst-free thermal evaporation or the simple chemical techniques involving not many complicated reactions might be the solution for the easy way to prepare ZnO nanostructures in large scale.

In this work, we report on the controlled synthesis of ZnO nanostructures with different morphologies using a simple low-temperature hydrothermal technique. Nanoparticles, nanorods, nanoflowers, and rectangular nanostructures of good crystallinity and composition were synthesized at low temperatures (80−100 °C) with excellent reproducibility. Scanning electron microscopy (SEM), X-ray diffraction (XRD), and transmission electron microscopy (TEM) and photoluminescence (PL) techniques were used to characterize the samples.

Experimental Section

In a typical synthesis process, 80 cm^3 of water and ethylenediamine (En) mixture (5 or 10 volume % of En) was poured into a double-neck 100-cm^3 round-bottom flux. The pH of the water and En mixtures were 13.5 for 10% En and 12.0 for 5% En. Zinc acetate dihydrate [$(CH_3COO)_2Zn{\cdot}2H_2O$] (Baker) crystals were added to the solvent until a desired pH is reached (Table 1) under vigorous agitation. After dissolving the zinc acetate completely, sodium hydroxide (99%, Aldrich) pellets were added to the mixture to increase the pH of the mixture to a desired value (Table 1). The mixtures were heated and kept between 80 and 100 °C for 2 h under steering. After cooling the mixtures to room temperature under steering, the white precipitates formed at the bottom of the reaction flux were filtered and washed several times by deionized water and dried at room temperature.

TABLE 1: Synthesis Parameters and Morphology of Different ZnO Nanostructures[a]

sample	En	pH_i	pH_f	morphology
ZnO-1	10%	8.6	11.0	elongated nanoparticles
ZnO-2	10%	9.0	11.0	flower like nanostructures
ZnO-3	10%	10.0	11.0	inhomogeneous nanorods
ZnO-4	10%	10.0	12.0	inhomogeneous nanorods
ZnO-5	10%	11.0	12.0	homogeneous nanorods of high aspect ratio
ZnO-6	5%	8.6	11.0	inhomogeneous nanorods
ZnO-7	5%	9.0	12.0	homogeneous nanorod bundles
ZnO-8	5%	10.0	12.0	homogeneous nanorods with low aspect ratio
ZnO-10	5%	8.6	12.0	defective nanoparticles, short nanorods, and rectangular nano-sheets

[a] All of the sample were synthesized between 80 and 100 °C, with 2 h reaction time.

Morphology of the samples were studied by a scanning electron microscope (JEOL JSM 5600LV, with Noarn analytical system attached) after dispersing them in water and spreading them on gold-coated stainless steel substrates. Monochromatic Cu Kα radiation from a Phillips (X'Pert) diffractometer was used for recording the diffraction pattern of the samples. A JEOL FEG 2010 FasTem electron microscope with 1.9-Å resolution (point to point) and high-angle annular dark-field detector attached was used for the fine structure study of the samples. A 210-nm radiation from a Ti:Sapphire laser (2 mW average beam power, focused to a 200-nm spot on the sample) was used for the room-temperature PL measurements.

* To whom correspondence should be addressed. E-mail: upal@sirio.ifuap.buap.mx. Fax: +52-222-2295611.
† Universidad Autónoma de Puebla.
‡ Universidad Nacional Autónoma de México.

10.1021/jp052496i CCC: $30.25
Published on Web 07/22/2005

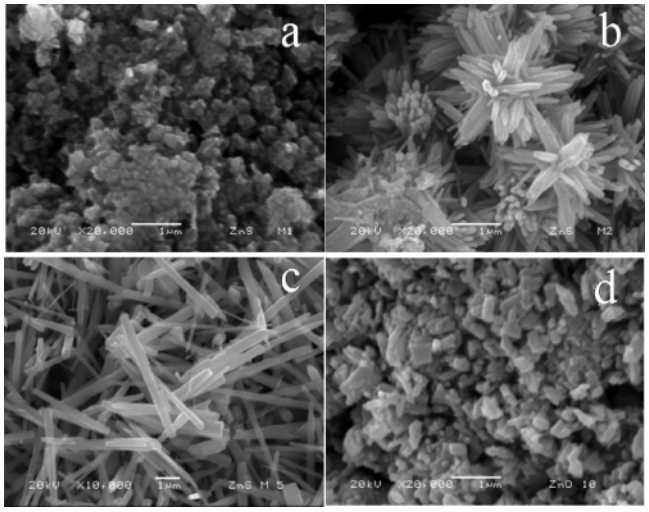

Figure 1. Typical SEM micrographs of the samples (a) ZnO-1, (b) ZnO-2, (c) ZnO-5, and (d) ZnO-10 with distinct morphologies. The scale bars in the micrographs represent 1 μm.

Results and Discussion

In Figure 1, the SEM micrographs of four typical samples with distinct morphologies are presented. While the Figure 1a shows the formation of ZnO nanoparticles of about 125 nm average size, formation of flowerlike nanorod bunches, uniform nanorods of about 170 nm average diameter and 2.5 μm average length, and particles with small nanorods can be observed in parts b, c, and d of Figure 1, respectively. While all these structures were synthesized almost at the same reaction temperature and either with 10% or 5% En contents, the pH and reactant content in the reaction mixture were different. It is important to mention that the structures were well reproducible when the growth parameters were kept unchanged. However, the size of the nanostructures could be varied to some extent by varying the reaction time. Though the real mechanism of formation of such morphologies is debatable,[22−25] we believe that, by changing the initial and final pH of the reaction mixture, we varied the rate of nucleation and growth events.[22] When the difference between the initial and final pH values is high, the nucleation rate is high; the formation of nanoparticle occurs at a faster rate and the supply of the precursors impinging on the particle surface ceases quickly. While the difference between the initial and final pH values is low, the nucleation rate is slow and the particles reaches to their critical size under the steady flow of precursors. When the area of c-face in the particle becomes larger than the critical size for island nucleation, further nucleation occurs on it and the process repeats to form nanorod structures.[26] For the intermediate difference in pH values, the nucleation rate is moderate and an anisotropic columnar growth may proceed by repeated nucleation and epitaxial growth at the top and side faces of the initial wurtzite structure.[25]

In Figure 2, the XRD spectra of the nanostructures synthesized at different initial and final pHs are presented. We can observe the formation of well crystalline hexagonal ZnO for all the samples, while the crystallinity of the samples increased on reducing the difference between the initial and final pH of the reaction mixture (as indicated by the increase of the XRD peak intensities). All the XRD peaks were indexed (Figure 2), and they agreed well with the standard ZnO of hexagonal structure (JCPDS 89-1397). Our EDS results revealed excellent stoichiometry for all the samples.

Figure 3 shows the high-resolution electron microscopy (HREM) images of the samples ZnO-1 and ZnO-5 along with their fast Fourier transforms (FFTs). The ZnO-1 sample, with nanoparticle morphology in SEM, revealed oval-shaped particles

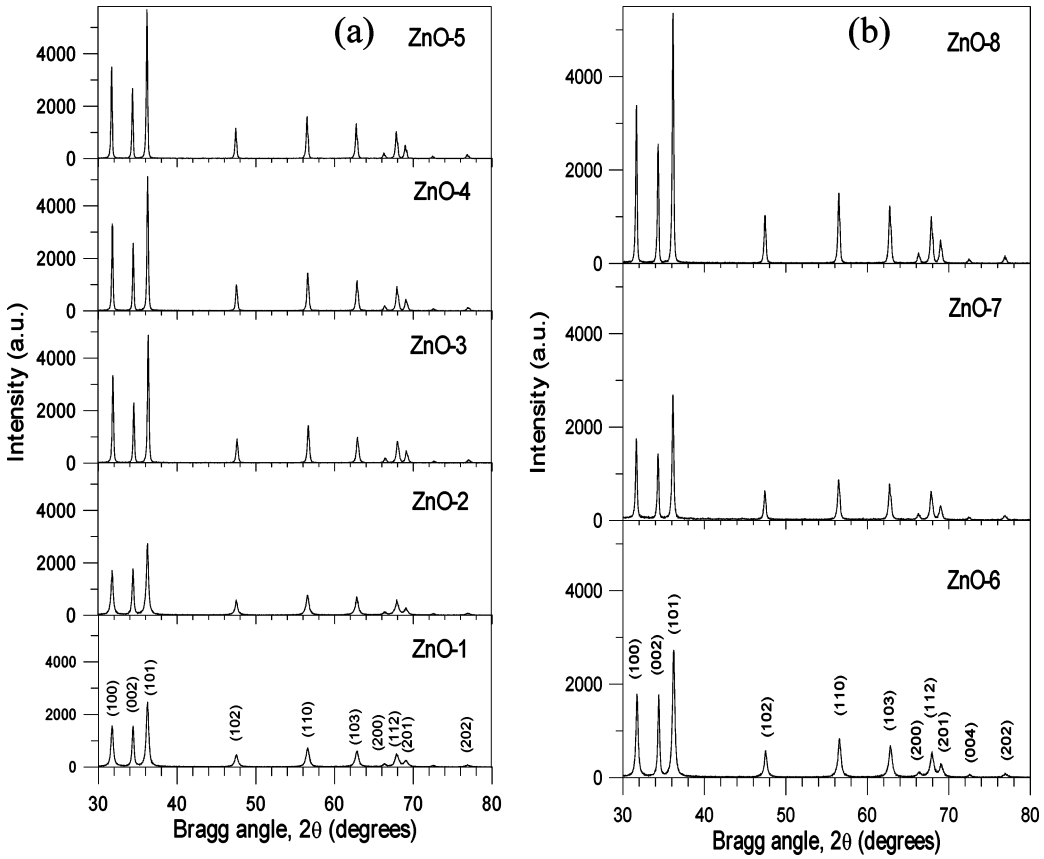

Figure 2. XRD patterns of the ZnO nanostructures grown with (a) 10% En and (b) 5% En. See sample details in Table 1.

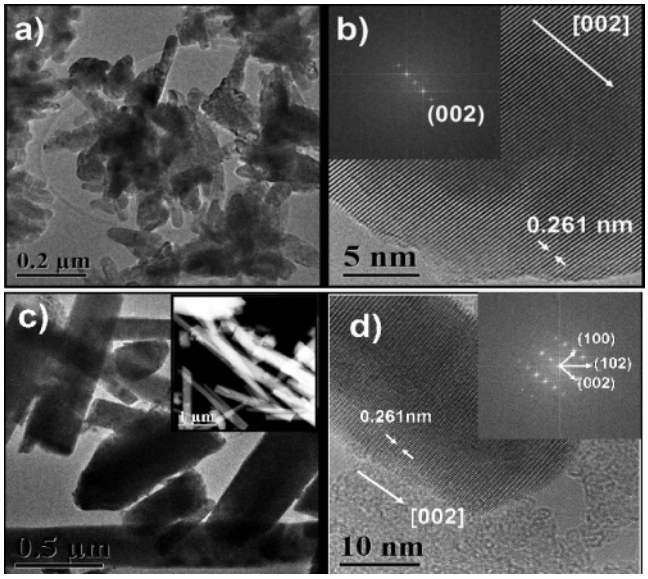

Figure 3. (a) Conventional TEM micrograph of sample ZnO-1, revealing oval and rodlike morphologies; (b) HREM micrograph of a rodlike structure of sample ZnO-1; (c) conventional low magnification TEM and HAADF images of sample ZnO-5, showing one-dimension structures of few micrometer lengths; (d) HREM micrograph of a nanorod of sample ZnO-5. The FFT of the corresponding HREM micrographs are shown as insets.

along with some rodlike structures in the low magnification TEM images (Figure 3a). While most of the nanoparticles revealed single-crystal structure (Figure 3b) with [002] growth direction, a few of them oriented differently. In the case of the ZnO-5 sample, synthesized with lower pH difference, all the rodlike nanostructures are of single crystal in nature and grown along the [002] direction. Estimated lattice parameter along the *c* axis for all the samples was 5.22 Å, which is very close to the lattice parameter of single-crystal wurtzite ZnO (5.206 Å), indicating a very low level of strain in the nanostructures.

In Figure 4, the TEM micrographs of the ZnO-2 sample are presented. For this sample, the growth kinetics revealed the formation of flowerlike structures consisting of conical nanorods and some fiberlike planer structures of about 1 μm average length. While most of the crystalline conical nanorods of homogeneous mass distribution (as observed from their HAADF images) grow along the [002] direction (Figure 4b), some of them grow along [101] (Figure 4c and 4d). On the other hand, the fiberlike planar structures revealed stacked layer configurations, where the stacking process is not always perfect, generating a rotation between the layers (Figure 4f). These fiberlike structures grow along [002] direction and produce Moire's fringes due to relative rotation of the stacked layers (Figure 4f).

The sample ZnO-10, synthesized with maximum difference between the initial and final pH values, produced nanostructures of several morphologies: nanoparticles of 30−70 nm diameter, small conical nanorods, and rectangular sheets (Figure 5). As in the case of ZnO-2, the planar structures consist of several stacked layers with faceted morphology. While the crystalline nanorods and nanosheets grow in wurtzite structure along [002] direction, surprisingly, the spherical particles grow in cubic phase. Moreover, most of the particles have etched-like central parts containing stacking faults (Figure 5c). The lattice parameters for these nanoparticles are estimated to be 2.8 and 1.98 A, correspond to the (111) and (211) planes of cubic ZnO (JCPDS 78-1124). As the sample was synthesized with highest difference between the initial and final pH values, we believe the nucleation and growth rate was fastest among the samples, causing a thermodynamically unstable condition for the growth of nanostructures of any particular morphology apart from generating stacking faults and strain fringes (Figure 5b) occasionally.

In Figure 6, the representative PL spectra of the samples are presented. In general, the room temperature PL spectra of all the as-grown and annealed samples revealed similar features. There appeared one sharp emission band at about 384 nm, generally assigned as a near-band-edge (NBE) emission band, and another broad deep-level emission band extending from 450 to 650 nm. The position of the NBE emission band in our nanostructures agrees well with the reported value for the nanowires grown by thermal evaporation.[21] On annealing in air at 250 °C for 1 h, while the intensity of the NBE band increased

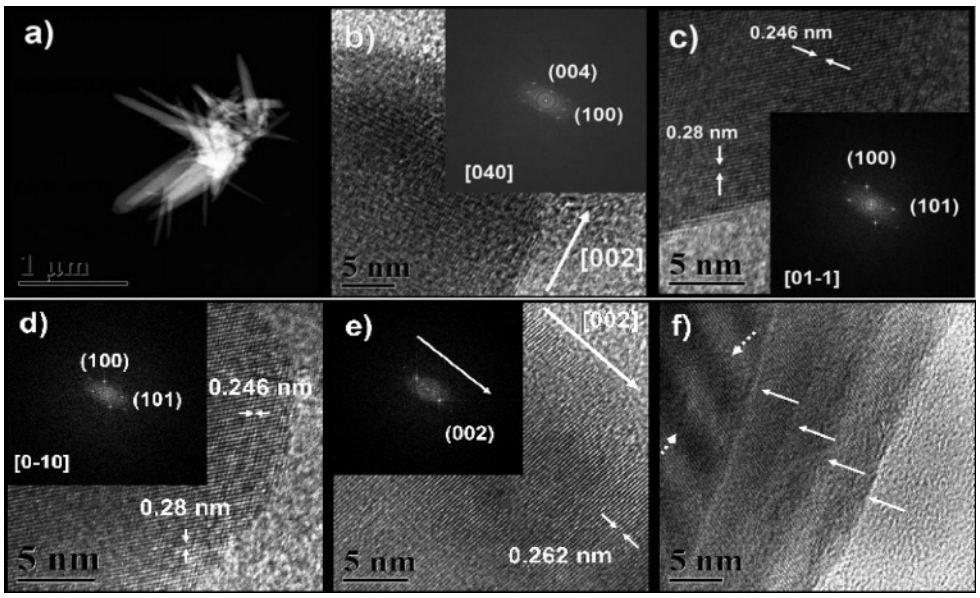

Figure 4. (a) Typical low-magnification HAADF image of ZnO-2 sample, showing flowerlike morphology; (b) HREM image of the tip of a conical nanorod grown along [002]; (c) lateral view of HREM image of a conical nanorod grown along [101] with its FFT; (d) HREM image of the tip of a nanorod grown along [101] with its FFT; (f) stacked layers (marked by arrows) growth of a planer nanostructure, showing rotation between the crystalline stacked layers. The Moire's patterns produced by such relative rotation are shown by dotted arrows.

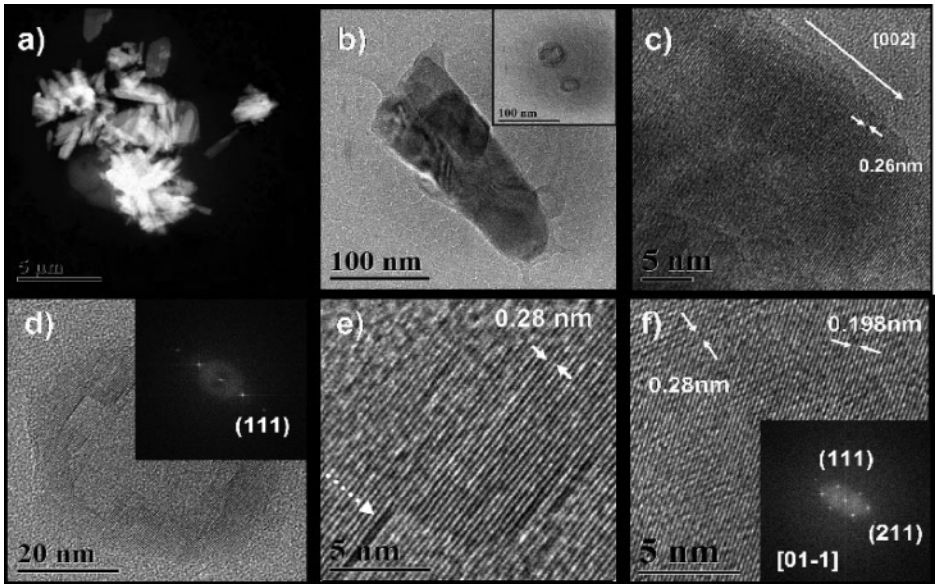

Figure 5. (a) Typical low-magnification HAADF image of ZnO-10 sample showing dense nanostructures of different morphologies; (b) short conical nanorod with spherical nanoparticles; (c) HREM image of a typical conical shape nanorod grown along [002]; (d) typical HREM of nanoparticles with etched-like center; (e) magnified HREM image of the same nanoparticle showing staking fault (dotted arrow); (f) HREM image of a nanoparticle showing lattice parameter of cubic phase. In d and f, the FFTs of the corresponding HREM images are shown in insets.

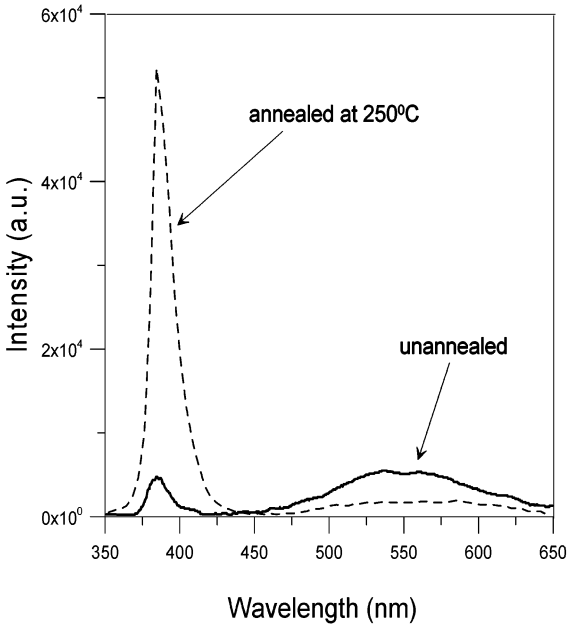

Figure 6. PL spectra of sample c (ref Figure 1) before and after thermal annealing at 250 °C for 1 h in air.

drastically without changing its position, the intensity of the broad deep-level emission band reduced, indicating a reduction of strain and deep-level defects on annealing, respectively. Generally, the deep-level emission in ZnO consists of a green emission around 520 nm and a near-yellow emission around 640 nm.[27,28] Though the origin of the green emission is controversial,[29−31] generally it is assigned to the singly ionized oxygen vacancies.[30,31] The yellow emission has been related to the interstitial O_i[−28,33,34] in ZnO. Therefore, the evolution of green and yellow bands in ZnO is competitive with each other. The broad emission band revealed in the visible region in our samples is due to the superposition of green and yellow emissions. On air annealing, the intensity ratio of deep-level emission and NBE emission ($I_{\text{deep-level}}/I_{\text{NBE}}$) decreased from 5.8 to about 0.22 due to annealing out of point defect and defect complexes. The evolution of these bands on thermal annealing in oxygen atmosphere is under study.

Conclusions

In conclusion, we could develop a simple low-temperature hydrothermal method to synthesize single crystalline, hexagonal ZnO nanostructures with different morphologies. By controlling the initial and final pH of the reaction mixture, ZnO nanostructures of different morphologies could be grown through controlling the nucleation and growth rates. The 1D nanostructures grow preferentially along the [002] *c* axis with low strain. The crystal quality of the nanostructures could further be improved through reduction of strain and deep-level defects by annealing them in air. Though several low-temperature chemical or hydrothermal synthesis of ZnO nanowires and nanoparticles have been reported recently,[17,18,35−37] our low-temperature synthesis method allows to synthesize ZnO nanostructures of several morphologies in a controlled manner.

Acknowledgment. We thank E. Aparecio Ceja, CCMC, UNAM, C. Magaña, IFUNAM for taking XRD traces and SEM micrographs of the samples respectively and L. Rendon for TEM work. We also acknowledge Dr. X. Gang, Wake Forest University, for his help in PL measurement of the samples. The work is partially supported by the VIEP-CONACyT-SEP Grant (No. II 194-04/EXC/I).

References and Notes

(1) Klingshirn, C. *Phys. Status Solidi B* **1975**, *71*, 547.
(2) Bagnall, D. M.; Chen, Y. F.; Zhu, Z.; Yao, T.; Koyama, S.; Shen, M. Y.; Goto, T. *Appl. Phys. Lett.* **1997**, *70*, 2230.
(3) Comini, E.; Fagila, G.; Sberveglieri, G.; Pan, Z.; Wang, Z. L. *Appl. Phys. Lett.* **2002**, *81*, 1869.
(4) Bai, X. D.; Gao, P. X.; Wang, Z. L.; Wang, E. G. *Appl. Phys. Lett.* **2003**, *82*, 4806.
(5) Xu, C. X.; Sun, X. W. *Appl. Phys. Lett.* **2003**, *83*, 380.
(6) Li, Q. H.; Wan, Q.; Chen, Y. J.; Wang, T. H.; Jia, H. B.; Yu, D. P. *Appl. Phys. Lett.* **2004**, *84*, 636.
(7) Ng, H. T.; Han, J.; Yamada, T.; Nguyen, P.; Chen, Y. P.; Meyyappan, M. *Nano Lett.* **2004**, *4*, 1247.
(8) Kind, H.; Yan, H.; Messer, B.; Mathew, L.; Yang, P. *Adv. Mater.* **2004**, *14*, 158.

(9) Ng, H. T.; Chen, B.; Li, J.; Han, J.; Meyyappan, M.; Wu, J.; Li, S. X.; Haller, E. E. *Appl. Phys. Lett.* **2003**, *82*, 2023.
(10) Yang, P.; Yan, H.; Mao, S.; Russo, R.; Johnson, J.; Saykally, R.; Morris, N.; Pham, J.; He, R.; Choi, H.-J. *Adv. Funct. Mater.* **2002**, *12*, 323.
(11) Lyu, S. C.; Zhang, Y.; Ruh, H.; Lee, H.-J.; Shim, H.-W.; Suh, E.-K.; Lee, C. J. *Chem. Phys. Lett.* **2002**, *363*, 134.
(12) Gao, P. X.; Wang, Z. L. *J. Phys. Chem. B* **2004**, *108*, 7534.
(13) Zhang, Y.; Jia, H.; Xuhubi, L.; Chen, X.; Yu, D.; Rongming, W. *J. Phys. Chem. B* **2003**, *107*, 8289.
(14) Roy, V. A. L.; Djurisic, A. B.; Chan, W. K.; Gao, J.; Lui, H. F.; Surya, C. *Appl. Phys. Lett.* **2003**, *83*, 141.
(15) Jiansheng, J.; Wang, G.; Wang, Q.; Chen, Y.; Han, X.; Wang, X.; Hou, J. G. *J. Phys. Chem. B* **2004**, *108*, 11976.
(16) Vayssieres, L. *Adv. Mater.* **2003**, *15*, 464.
(17) Wang, J.; Gao, L. *J. Mater. Chem.* **2003**, *13*, 2551.
(18) Liu, B.; Zeng, H. C. *J. Am. Chem. Soc.* **2003**, *125*, 4430.
(19) Li, Y.; Meng, G. W.; Zhang, L. D. *Appl. Phys. Lett.* **2000**, *76*, 2011.
(20) Zheng, M. J.; Zhang, L. D.; Li, G. H.; Shen, W. Z. *Chem. Phys. Lett.* **2002**, *363*, 123.
(21) Lee, W.; Jeong, M.-C.; Myoung, J.-M. *Nanotechnology* **2004**, *15*, 1441.
(22) Li, W.-J.; Shi, E.-W.; Zhong, W.-Z.; Yin, Z.-W. *J. Cryst. Growth* **1999**, *203*, 186.
(23) Wander, A.; Harrison, N. M. *Surf. Sci.* **2000**, *468*, L851.
(24) Donnay, J. D. H.; Harker, D. *Am. Miner.* **1937**, *22*, 446.
(25) Baxter, J. B.; Wu, F.; Ayudil, E. S. *Appl. Phys. Lett.* **2003**, *83*, 3797.
(26) Tersoff, J.; Vandergon, A. W. D.; Tromp, R. M. *Phys. Rev. Lett.* **1994**, *72*, 266.
(27) Ong, H. C.; Du, G. T. *J. Cryst. Growth* **2004**, *265*, 471.
(28) Studenikin, S. A.; Golego, N.; Cocivera, M. *J. Appl. Phys.* **1998**, *84*, 2287.
(29) Lin, B.; Fu, Z.; Jia, Y. *Appl. Phys. Lett.* **2001**, *79*, 943.
(30) Vanheusden, K.; Warren, W. L.; Seager, C. H.; Tallant, D. R.; Voigt, J. A.; Gnade, B. E. *J. Appl. Phys.* **1996**, *79*, 7983.
(31) Osaga, K.; Sakurai, K.; Fujita, S.; Fujita, S.; Matsushige, K. *J. Cryst. Growth* **2000**, *214*/*215*, 312.
(32) Li, W.; Mao, D.; Zhang, F.; Wang, X.; Liu, X.; Zou, S.; Zou, Y.; Li, Q.; Xu, J. *Nucl. Instrum. Methods Phys. Res. B* **2000**, *169*, 53.
(33) Liu, M.; Kitai, A. H.; Mascher, P. *J. Lumin.* **1992**, *54*, 35.
(34) Wu, X. L.; Siu, G. G.; Fu, C. L.; Ong, H. C. *Appl. Phys. Lett.* **2001**, *78*, 2285.
(35) Menulenkamp, E. A. *J. Phys. Chem. B* **1998**, *102*, 5566.
(36) Koh, Y. W.; Lin, M.; Tan, C. K.; Foo, Y. L.; Loh, K. P. *J. Phys. Chem. B* **2004**, *108*, 11419.
(37) Zhang, H.; Yang, D.; Ji, Y.; Ma, X.; Xu, J.; Que, D. *J. Phys. Chem. B* **2004**, *108*, 3955.